Optics Communications 356 (2015) 155–160

Contents lists available at ScienceDirect

Optics Communications

journal homepage: www.elsevier.com/locate/optcom

Controllable cavity linewidth narrowing via spontaneously generated coherence in a four level atomic system

Si-Cong Tian [a], Ren-Gang Wan [b], Xiao-Nan Shan [a], Cun-Zhu Tong [a,*], Li Qin [a], Yong-Qiang Ning [a]

[a] State Key Laboratory of Luminescence and Applications, Changchun Institute of Optics, Fine Mechanics and Physics, Chinese Academy of Sciences, Changchun 130033, China
[b] School of Physics and Information Technology, Shanxi Normal University, Xi'an 710062, China

ARTICLE INFO

Article history:
Received 29 October 2014
Received in revised form
24 July 2015
Accepted 26 July 2015

Keywords:
Intracavity electromagnetically induced transparency
Cavity linewidth narrowing
Spontaneously generated coherence

ABSTRACT

A scheme for cavity linewidth narrowing in a four-level atomic system with spontaneously generated coherence is proposed. The atomic system consists of three closely spaced excited levels, which decay to one common ground level. In such a system, spontaneously generated coherence can result in the appearance of two narrow transparency windows accomplished by steep normal dispersion. When the medium is embedded in a ring cavity, two ultranarrow transmission peaks locating close to the position of the transparency windows can be obtained simultaneously. The cavity linewidth narrowing is owing to the quantum interference between the three decay channels and can be controlled by the frequency splitting of the excited levels, requiring no coupling lasers.

1. Introduction

The phenomenon of electromagnetically induced transparency (EIT), which is a result of dynamically induced coherence (DIC), plays an important role in the interaction between light and matter [1,2]. EIT can lead to many applications such as light propagation control [3,4], light storage [5], enhancement of nonlinearity at low light levels [6], etc. Steep dispersion and almost vanishing absorption produced by EIT can induce cavity-linewidth narrowing, which is known as intracavity EIT termed by Lukin et al. [7], and was first experimentally observed in a hot atomic vapor [8], then in a cold atomic system [9], in a Doppler broadened medium [10] and in a four-level tripod atomic system [11]. Intracavity EIT can be used for higher resolution spectroscopic measurements and frequency stabilization [7], and contributes to slowdown and delay of the light pulse propagation [12].

The above studies on the intracavity EIT are all based on the laser induced atomic coherence in an atomic system, and it is crucial to have at least one coupling laser to create the necessary coherence. On the other hand, atomic coherence can also be created through spontaneous emission in certain media if relevant decay pathways are correlated via the same vacuum modes, which is defined as spontaneously generated coherence (SGC). SGC gives rise to a variety of quantum effects, such as narrowing and quenching of spontaneous emission [13–19], amplification without inversion [20–23], transparency of a laser field [24,25] and modifying of nonlinearity [26–32] (optical bistability (OB) [26–30], enhancing Kerr nonlinearity [31] and electromagnetically induced grating [32]). Other novel applications of using SGC are the field of quantum photocell [33], high-precision metrology [34] and quantum heat energy [35].

And recently, the resonance fluorescence, the squeezing and the absorption spectra of a four-level atomic system with SGC have been investigated [36]. And in a similar atomic system, the existence of SGC can lead to the double-dark states [37]. Inspired by these works, in this paper, we propose a scheme for obtaining a tunable ultranarrow cavity transmission in a four-level atomic system consisting of three closely spaced excited levels decaying to one common ground level. In such a system, SGC can result in two narrow transparency windows and steep dispersion. And close to the narrowed transparency windows, two ultranarrow cavity transmission peaks can be obtained simultaneously, which can support frequency stabilization of two lasers with different central frequencies. In contrast to the previous studies, the cavity linewidth narrowing obtained in our scheme is due to the decay-induced interference, and no coupling laser is required.

Note that SGC only exists in such a system, which has near-degenerated levels and non-orthogonal dipole matrix elements. That is to say, the closely spaced levels should have the same quantum numbers J and m_J [20]. However, these rigorous

* Corresponding author. Fax: +86 431 861 76020.
E-mail addresses: tiansicong@ciomp.ac.cn (S.-C. Tian), tongcz@ciomp.ac.cn (C.-Z. Tong).

http://dx.doi.org/10.1016/j.optcom.2015.07.068
0030-4018/

conditions are rarely met in real atoms, therefore no experimental work has been carried out in atomic systems to observe SGC directly. However, SGC can be realized in other systems. For example, cavity field [38], anisotropy vacuum [39], photonic crystals [40] and left-handed materials [41] can result in quantum interference even when the dipole moments of the decay channels are orthogonal. And SGC can also be simulated in the dressed atoms interacting with a dc field [42], microwave field [43,44] or laser field [45]. And most recently, by the coherent laser fields we experimentally observed SGC on absorption and fluorescence in rubidium atomic beam [46–48]. Besides, in quantum wells and quantum dots, the tunneling effect can also lead to quantum interference [49–52]. Therefore, although our scheme proposed here is difficult to be carried out with atoms in a free vacuum, it can be equally applied and achieved with the above systems.

The paper is organized as follows: in Section 2, the model and the basic equations are introduced. In Section 3, the absorption and dispersion spectra are plotted. In Section 4, the transmission spectrum is plotted. Section 5 is the conclusions.

2. Models and equations

We consider a four-level atomic system as shown in Fig. 1(a). It has three excited levels $|2\rangle$, $|3\rangle$ and $|4\rangle$, which are coupled by the same vacuum modes to the ground level $|1\rangle$. $E_i = \hbar\omega_i$, $(i = 2, 3, 4)$ is the energy of the excited levels $|i\rangle$, with ω_i being the frequency of the corresponding level (We have taken the ground level $E_1 = 0$ as the energy origin). And $\omega_{32} = \omega_3 - \omega_2$ and $\omega_{43} = \omega_4 - \omega_3$ are the frequency splitting of level $|2\rangle$ and $|3\rangle$, and that of level $|3\rangle$ and $|4\rangle$, respectively. Then we suppose a weak probe field with frequency ω_p scanning over the system. The probe field probes on all transitions $|1\rangle \leftrightarrow |2\rangle$, $|1\rangle \leftrightarrow |3\rangle$ and $|1\rangle \leftrightarrow |4\rangle$ simultaneously. The Rabi frequencies for each transition is $\Omega_2 = E_p\mathbf{e}_p\cdot\boldsymbol{\mu}_{12}/2\hbar$, $\Omega_3 = E_p\mathbf{e}_p\cdot\boldsymbol{\mu}_{13}/2\hbar$, and $\Omega_4 = E_p\mathbf{e}_p\cdot\boldsymbol{\mu}_{14}/2\hbar$, where E_p and $\mathbf{e}_p$ are the amplitude and the polarization vector of the probe field, and $\boldsymbol{\mu}_{12}$, $\boldsymbol{\mu}_{13}$ and $\boldsymbol{\mu}_{14}$ are the dipole moments of the respective transitions. The polarization direction of the probe field and the dipole moments are shown in Fig. 1(b). And the detuning between the $|1\rangle \leftrightarrow |i\rangle (i = 2, 3, 4)$ transition and the probe field is $\Delta_i = \omega_i - \omega_p$. Let $\Delta_3 = \Delta_p$, then $\Delta_2 = \Delta_p - \omega_{32}$ and $\Delta_4 = \Delta_p + \omega_{43}$.

The Hamiltonian for the interaction between the atom and the laser in the frame rotating with $\Omega_i (i = 2, 3, 4)$ takes the form [13]

$$H = (\Delta_p - \omega_{32})\sigma_{22} + \Delta_p\sigma_{33} + (\Delta_p + \omega_{43})\sigma_{44} + [(\Omega_2\sigma_{12} + \Omega_3\sigma_{13} + \Omega_4\sigma_{14}) + H.c.]. \quad (1)$$

Here $\sigma_{ij} = |i\rangle\langle j|$ represents a population operator for $i = j$ and a dipole transition operator for $i \neq j$. And direct transitions between the excited sublevels $|i\rangle (i = 2, 3, 4)$ are dipole forbidden. And we use units such that $\hbar = 1$.

Assuming that such an atomic system is damped by the standard vacuum, the master equation for the reduced density operator ρ of the atom in the rotating frame then takes the form [13]

$$\frac{d\rho}{dt} = -i[H, \rho] + \frac{1}{2}L\rho, \quad (2)$$

with

$$\begin{aligned} L = {} & \gamma_2(2\sigma_{12}\rho\sigma_{21} - \sigma_{22}\rho - \rho\sigma_{22}) \\ & + \gamma_3(2\sigma_{13}\rho\sigma_{31} - \sigma_{33}\rho - \rho\sigma_{33}) \\ & + \gamma_4(2\sigma_{14}\rho\sigma_{41} - \sigma_{44}\rho - \rho\sigma_{44}) \\ & + \gamma_{23}(2\sigma_{13}\rho\sigma_{21} - \sigma_{23}\rho - \rho\sigma_{23}) + \gamma_{23}(2\sigma_{12}\rho\sigma_{31} - \sigma_{32}\rho - \rho\sigma_{32}) \\ & + \gamma_{24}(2\sigma_{14}\rho\sigma_{21} - \sigma_{24}\rho - \rho\sigma_{24}) + \gamma_{24}(2\sigma_{12}\rho\sigma_{41} - \sigma_{42}\rho - \rho\sigma_{42}) \\ & + \gamma_{34}(2\sigma_{14}\rho\sigma_{31} - \sigma_{34}\rho - \rho\sigma_{34}) + \gamma_{34}(2\sigma_{13}\rho\sigma_{41} - \sigma_{43}\rho - \rho\sigma_{43}). \end{aligned} \quad (3)$$

Her γ_2, γ_3 and γ_4 are the spontaneous decay rates from the three excited levels to the ground level, respectively. And γ_{23}, γ_{24} and γ_{34} represent the SGC effect between the three excited levels, and can be written as [24,36,42]

$$\gamma_{ij} = p_{ij}\frac{\sqrt{\gamma_i\gamma_j}}{2}, \quad (i, j = 2, 3, 4;\ i \neq j). \quad (4)$$

Here $p_{ij} = \cos\theta_{ij}$, $(i, j = 2, 3, 4;\ i \neq j)$ measures the degree of SGC, with θ_{ij} being the angle between the two transition dipole moments $\boldsymbol{\mu}_{1i}$ and $\boldsymbol{\mu}_{1j}$. If $\boldsymbol{\mu}_{1i}$ and $\boldsymbol{\mu}_{1j}$ are parallel, then $p_{ij} = 1$ ($\theta_{ij} = 0^\circ$) and SGC takes the maximum value, while if $\boldsymbol{\mu}_{1i}$ and $\boldsymbol{\mu}_{1j}$ are perpendicular, then $p_{ij} = 0$ ($\theta_{ij} = 90^\circ$) and SGC disappears.

Then the equations of the time evolution of the reduced density matrix elements take the form

$$\dot{\rho}_{22} = i\Omega_2(\rho_{12} - \rho_{21}) - \gamma_{23}(\rho_{23} + \rho_{32}) - \gamma_{24}(\rho_{24} + \rho_{42}) - \gamma_2\rho_{22}, \quad (5a)$$

$$\dot{\rho}_{33} = i\Omega_3(\rho_{13} - \rho_{31}) - \gamma_{23}(\rho_{23} + \rho_{32}) - \gamma_{34}(\rho_{34} + \rho_{43}) - \gamma_3\rho_{33}, \quad (5b)$$

$$\dot{\rho}_{44} = i\Omega_4(\rho_{14} - \rho_{41}) - \gamma_{24}(\rho_{24} + \rho_{42}) - \gamma_{34}(\rho_{34} + \rho_{43}) - \gamma_4\rho_{44}, \quad (5c)$$

$$\dot{\rho}_{12} = -i\Omega_2(\rho_{22} - \rho_{11}) + i\Omega_3\rho_{32} + i\Omega_4\rho_{42} - \gamma_{23}\rho_{13} - \gamma_{24}\rho_{14} + [-\frac{\gamma_2}{2} + i(\Delta_p - \omega_{32})]\rho_{12}, \quad (5d)$$

$$\dot{\rho}_{13} = -i\Omega_3(\rho_{33} - \rho_{11}) + i\Omega_2\rho_{23} + i\Omega_4\rho_{43} - \gamma_{23}\rho_{12} - \gamma_{34}\rho_{14} + (-\frac{\gamma_3}{2} + i\Delta_p)\rho_{13}, \quad (5e)$$

$$\dot{\rho}_{14} = -i\Omega_4(\rho_{44} - \rho_{11}) + i\Omega_2\rho_{24} + i\Omega_3\rho_{34} - \gamma_{24}\rho_{12} - \gamma_{34}\rho_{13} + [-\frac{\gamma_4}{2} + i(\Delta_p + \omega_{43})]\rho_{14}, \quad (5f)$$

$$\dot{\rho}_{23} = i\Omega_2\rho_{13} - i\Omega_3\rho_{21} - \gamma_{23}(\rho_{22} + \rho_{33}) - \gamma_{24}\rho_{43} - \gamma_{34}\rho_{24} + (-\frac{\gamma_2 + \gamma_3}{2} - i\omega_{32})\rho_{23}, \quad (5g)$$

$$\dot{\rho}_{24} = i\Omega_2\rho_{14} - i\Omega_4\rho_{21} - \gamma_{24}(\rho_{22} + \rho_{44}) - \gamma_{23}\rho_{34} - \gamma_{34}\rho_{23} + [-\frac{\gamma_2 + \gamma_4}{2} + i(\omega_{32} + \omega_{43})]\rho_{24}, \quad (5h)$$

$$\dot{\rho}_{34} = i\Omega_3\rho_{14} - i\Omega_4\rho_{31} - \gamma_{34}(\rho_{33} + \rho_{44}) - \gamma_{23}\rho_{24} - \gamma_{24}\rho_{32} + (-\frac{\gamma_3 + \gamma_4}{2} + i\omega_{43})\rho_{23}. \quad (5i)$$

The above equations are constrained by $\rho_{11} + \rho_{22} + \rho_{33} + \rho_{44} = 1$ and $\rho_{ij} = \rho_{ji}^*$. And it should be emphasized that the interference terms in Eqs. (5a)–(5i) are significant only for small frequency

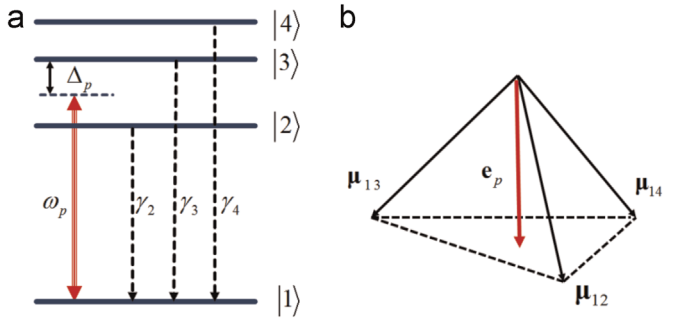

Fig. 1. (a) A four-level atomic system with SGC. (b) The arrangement of the probe field polarization and dipole moments of the transitions.

splitting between the three excited levels. Otherwise the SGC effect vanishes because that the oscillatory terms will average out to zero.

The probe field acts on all transitions, therefore the linear susceptibility χ is proportional to the sum of the density matrix element ρ_{12}, ρ_{13} and ρ_{14}. By solving Eqs. (5a)–(5i), one can obtain the expression of density matrix element ρ_{12}, ρ_{13} and ρ_{14}. For simplicity, we assume the dipole moment of the excited levels to ground level to be equal in magnitude and the angles between each other are the same as well, then we have $|\boldsymbol{\mu}_{12}| = |\boldsymbol{\mu}_{13}| = |\boldsymbol{\mu}_{14}| \equiv |\boldsymbol{\mu}|$, $\gamma_{12} = \gamma_{13} = \gamma_{14} \equiv \gamma$, $p_{23} = p_{24} = p_{34} \equiv p$ and $\gamma_{23} = \gamma_{24} = \gamma_{34} \equiv p\frac{\gamma}{2}$. We further assume that the angles between $\mathbf{e}_p$ and each of the dipoles are equal, thus we have $\Omega_2 = \Omega_3 = \Omega_4 \equiv \Omega$. Then in the condition of weak laser field, ρ_{11} is nearly equal to unity and $\rho_{22} \approx \rho_{33} \approx \rho_{44} \approx 0$. Then keeping the terms to the first order in the field Ω, the expression of $\rho_{12} + \rho_{13} + \rho_{14}$ is

$$\rho_{12} + \rho_{13} + \rho_{14} = \frac{\Omega\left[\frac{1}{(1-p+A)} + \frac{1}{(1-p+B)} + \frac{1}{(1-p+C)}\right]}{1 + p\left[\frac{1}{(1-p+A)} + \frac{1}{(1-p+B)} + \frac{1}{(1-p+C)}\right]}, \tag{6}$$

with

$$A = 2i(\Delta_p - \omega_{32})/\gamma, \tag{7a}$$

$$B = 2i\Delta_p/\gamma, \tag{7b}$$

$$C = 2i(\Delta_p + \omega_{43})/\gamma. \tag{7c}$$

Then the linear susceptibility χ is

$$\chi = \frac{4\pi N|\boldsymbol{\mu}|^2}{\Omega}(\rho_{12} + \rho_{13} + \rho_{14}) = \frac{4\pi N|\boldsymbol{\mu}|^2\left[\frac{1}{(1-p+A)} + \frac{1}{(1-p+B)} + \frac{1}{(1-p+C)}\right]}{1 + p\left[\frac{1}{(1-p+A)} + \frac{1}{(1-p+B)} + \frac{1}{(1-p+C)}\right]}, \tag{8}$$

where N is the medium density. The linear susceptibility χ can be separated into real (χ') and imaginary (χ'') parts, which represent the absorption and dispersion of the medium, respectively.

3. Absorption and dispersion spectra

In this part we plot in Fig. 2 the absorption (χ'') and dispersion (χ') spectra according to Eq. (8) for different parameters. First, we show in Fig. 2(a) for the case of $p = 0$, which means there is no SGC effect. From the figure one can see that there is one broad absorption peak (solid line) and a gentle dispersion curve (dotted line) in the spectrum. Then we consider the case of $p = 1$, indicating that the SGC effect takes maximum value. As can be seen from Fig. 2(b), two deep transparency windows appear in the absorption spectrum for $\omega_{32} = \omega_{43} = 0.5$. And within the transparency windows, there are two dispersion curves with the same positive slope.

Next we fix $p = 1$ (the case of maximal SGC effect), and see how the frequency splittings modify the absorption and dispersion spectra. When both ω_{32} and ω_{43} are reduced to 0.1, the width of the two transparency windows becomes much narrower, and both transparency windows move to the center of the absorption spectrum. And within the narrower transparency windows, two same steeper dispersion curves show up [Fig. 2(c)]. Then when only one frequency splitting is reduced, the absorption spectrum becomes unsymmetrical, with one broad transparency window and one narrow transparency window [Fig. 2(c)]. And the position of the narrow one is placed close to the center of the absorption spectrum. Within the narrow transparency window, the slope of the dispersion curve is much larger.

From Fig. 2, one can conclude that SGC is responsible for the appearance of the transparency windows. Furthermore, the frequency splitting of the excited levels can modify the width and the position of the transparency windows. The smaller value of frequency splitting will result in the narrower width of the transparency windows and steeper dispersion, and simultaneously make the transparency windows be closer to the center of the absorption spectrum. In the following, we will give an explanation for these results.

First we show how SGC results in the transparency windows. When there is no SGC effect ($p = 0$), Eq. (8) is reduced to

$$\chi = 4\pi N|\boldsymbol{\mu}|^2\left(\frac{1}{1+A} + \frac{1}{1+B} + \frac{1}{1+C}\right). \tag{9}$$

From Eq. (9), χ can not be zero for the near resonance situation, as a result we obtain one broad absorption peak without transparency window [Fig. 2(a)]. While in the case of the maximal SGC effect ($p = 1$), the linear susceptibility can go to zero if the laser frequency is tuned such that [36]

$$\omega_{\pm} = \frac{\omega_{43} - \omega_{32} \pm \sqrt{\omega_{32}^2 + \omega_{43}^2 + \omega_{32}\omega_{43}}}{3}. \tag{10}$$

Eq. (10) means that there are two transparency windows locating at the position of $\omega_{\pm}$ [Fig. 2(b)–(d)]. So the SGC effect (measured by the value of p) is responsible for the appearance of the transparency windows.

Second we show the dependence of the transparency windows

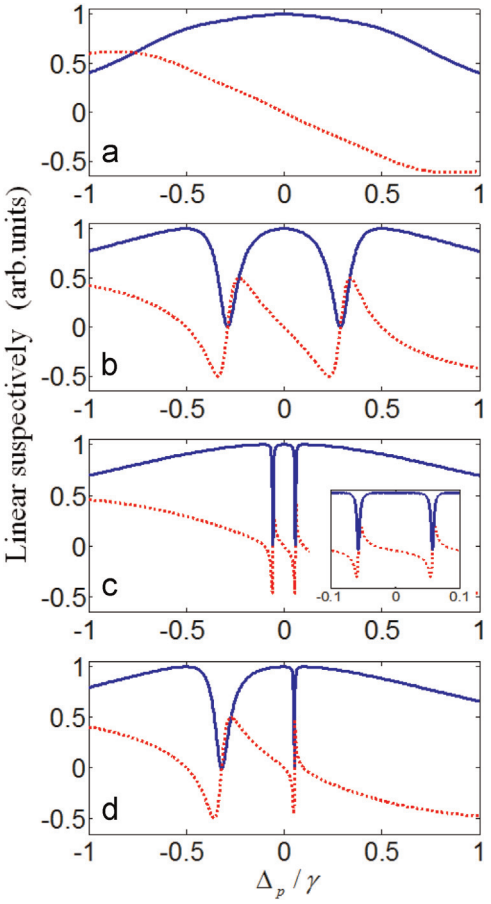

Fig. 2. The absorption spectrum (solid line) and dispersion spectrum (dotted line) as a function of Δ_p. The parameters are (a) $p = 0$, $\omega_{32} = \omega_{43} = 0.5$, (b) $p = 1$, $\omega_{32} = \omega_{43} = 0.5$, (c) $p = 1$, $\omega_{32} = \omega_{43} = 0.1$, and (d) $p = 1$, $\omega_{32} = 0.1$, $\omega_{43} = 0.5$. Other parameters are $\Omega = 0.01$, $\gamma = 1$. And all the parameters are scaled by γ.

position on the frequency splitting of the excited levels for $p = 1$. From Eq. (10), the transparency windows locate at the position of $\omega_{\pm}$, which can be modified by the frequency splitting. For example, in the symmetrical configuration of the three excited levels ($\omega_{32} = \omega_{43}$), two transparency windows are symmetrically placed at the position of $\omega_{\pm} = \pm\omega_{43}/\sqrt{3}$. And the smaller frequency splitting will result in the closer transparency windows, which is in agreement with Fig. 2(b) and (c).

Third we interpret the changing of the width of the transparency windows via frequency splitting. For $p = 1$ and considering the case of $\omega_{32} = \omega_{43}$, the imaginary part of χ is approximated to [36]

$$\mathrm{Im}(\chi) \approx 4\pi N|\mu|^2\left\{\frac{2\gamma^2}{\gamma^2+\Delta_p^2} - \frac{2(\omega_{43}/4)^2}{(\omega_{43}/4)^2+\left[\Delta_p-(\omega_{43}/\sqrt{3})\right]^2} - \frac{2(\omega_{43}/4)^2}{(\omega_{43}/4)^2+\left[\Delta_p+(\omega_{43}/\sqrt{3})\right]^2}\right\}. \tag{11}$$

Eq. (11) indicates that the absorption spectrum consists of three Lorentzians peaks, and the negative weights of the last two parts of the equation are responsible for the appearance of the two transparency windows. The widths of the transparency windows represented by the Lorentzians with negative weights are proportional to the frequency splitting, therefore the transparency windows can be made very narrow by reducing the frequency splitting [Fig. 2(c)]. When $\omega_{32} \neq \omega_{43}$, the expression for $\mathrm{Im}(\chi)$ is more complicated, however it can be inferred that the narrower transparency window is also due to the smaller value of frequency splitting [Fig. 2(d)].

Last we explain the changing of the dispersion by frequency splitting. Using Eq. (8), the slope of the real part of the linear susceptibility χ' within the transparency windows is

$$\left.\frac{\partial\chi'}{\partial\omega_p}\right|_{\omega_p=\omega_{\pm}} = \frac{2\gamma^2(3\omega_{\pm}+\omega_{32}-\omega_{43})}{\omega_{\pm}^2(2\omega_{\pm}+\omega_{32}-\omega_{43})}. \tag{12}$$

From Eq. (12), the slope of the dispersive curve within the transparency windows is steeper as the frequency splitting is decreased. For instance, when $\omega_{32} = \omega_{43}$, the two slopes of the dispersion are equal ($9\gamma^2/\omega_{43}^2$), which is in agreement with Fig. 2 (b) and (c).

To obtain more general case, we plot in Fig. 3 the three dimensional absorption and dispersion spectra for various value of frequency splitting ω_{32} and ω_{43} for $p = 1$. When $\omega_{32} = \omega_{43}$, the absorption spectrum is always symmetrical with two transparency windows. And with decreasing value of frequency splitting, the width of the two transparency windows becomes narrowing, and at the same time the position of them is moving to the center of the spectrum [Fig. 3(a)]. Then we fix the value of ω_{32} to small value ($\omega_{32} = 0.1$), and change the value of ω_{43}. From Fig. 3(c) one can see that the absorption spectrum is unsymmetrical. The width of one transparency window is kept narrowed, and the position of it is unchanged. As ω_{43} goes small, the width of the other transparency window is also narrowed and moves to the center of the spectrum. And in both cases, within the narrowed transparency windows, steep dispersion can be obtained [Fig. 3(b) and (d)].

4. Transmission spectrum

In this part we embed the atomic sample in a ring cavity, as shown in Fig. 4. The length of the optical cavity is L and the length of the sample is l. The cavity transmission can be expressed as [7]

$$S(\omega) = \frac{t^2}{1+r^2\kappa^2-2r\kappa\cos[\Phi(\omega)]}. \tag{13}$$

Here t and r are the transmissivity and the reflectivity of both the input and the output mirrors, respectively. For simplicity, mirror 3 is assumed to have 100% reflectivity, then we have $r^2 + t^2 = 1$. $\Phi(\omega) = \frac{\omega}{c}(L + l\chi')$ is the total phase shift, which is caused by the real part (χ') of the susceptibility (c is the velocity of the light in vacuum). And $\kappa = \exp(-\frac{\omega}{c}l\chi'')$ is the medium absorption per round trip, which is contributed by the imaginary part (χ'') of the susceptibility, leading to the attenuation of the amplification of the probe field.

On inspection of the round-trip phase shift, the pulling equation representing the resonance frequency of the combined cavity and medium system is [7]

$$\omega_r = \frac{1}{1+\eta}\omega_c + \frac{\eta}{1+\eta}\omega_p, \tag{14a}$$

$$\eta = \omega_p\frac{l}{2L}\frac{\partial\chi'}{\partial\omega_p}. \tag{14b}$$

Here η defines a frequency-locking or stabilization coefficient, which is dependence on the dispersion of the sample. Eqs. (14a) and (14b) indicates that ω_r is contributed by two factors, one is the resonance frequency of the empty cavity ω_c, with $\omega_c = mc/L$ (for integer m), and the other is the probe transition frequency ω_p. When ω_p is tuned to $\omega_{\pm}$ [Eq. (10)], the absorption goes to zero and the slope of the dispersion close to $\omega_{\pm}$ is steep. Therefore the medium around transparency window will pull the resonance frequency $\omega_r - \omega_{\pm}$, where transparency windows appear. And the steeper the dispersion is, the larger the frequency pulling effect is, and the better frequency stabilization effect is.

The width of cavity resonances $\delta\omega$ changed by the intracavity medium can be calculated by the methods used in Ref. [7],

$$\delta\omega = \frac{1-r\kappa}{\sqrt{\kappa}(1-r)}\frac{1}{1-\eta}\delta\omega_c, \tag{15}$$

where $\delta\omega_c$ is the empty-cavity linewidth. And $(1-r\kappa)/\sqrt{\kappa}(1-r)$ describes an enhancement of the effective cavity and medium width due to additional losses, while $1/(1-\eta)$ describes the reduction due to the linear dispersion. When $\omega_p = \omega_{\pm}$, the transparency of the probe field is induced, therefore the absorption can be negligible ($\chi'' \to 0$), whereas the dispersion is large. Then Eq. (15) can be simplified as

$$\delta\omega = \frac{1}{1-\eta}\delta\omega_c. \tag{16}$$

Eq. (16) indicates that the steep dispersion will result in substantial line narrowing within the transparency windows. From Eq. (12), the small frequency splitting will result in the steep dispersion, and thereby make the linewidth of the cavity transmission narrowed.

According to Eq. (13), we plot the cavity transmission spectrum in Fig. 5 with the same parameters used in Fig. 2. And for simplicity, we set the absorption cross-section as $\sigma = 4\pi\omega_p|\mu|^2/c\gamma$ [49], and thereby the propagation constant $N\sigma l$ is appreciable, i.e., $N\sigma l = 0.5$.

First, in the case of the minimum SGC effect ($p = 0$), there is no transmission peak, as shown in Fig. 5(a). The strong absorption in Fig. 2(a) is responsible for this result. Then we show in Fig. 5(b)–(d) the case of the maximum SGC effect ($p = 1$). When $\omega_{32} = \omega_{43} = 0.5$, one can see that the transmission spectrum is symmetrical with two same wide transmission peaks, as shown in Fig. 5(b). With reduced value of the frequency splitting ($\omega_{32} = \omega_{43} = 0.1$), the linewidth of the two transmission peaks

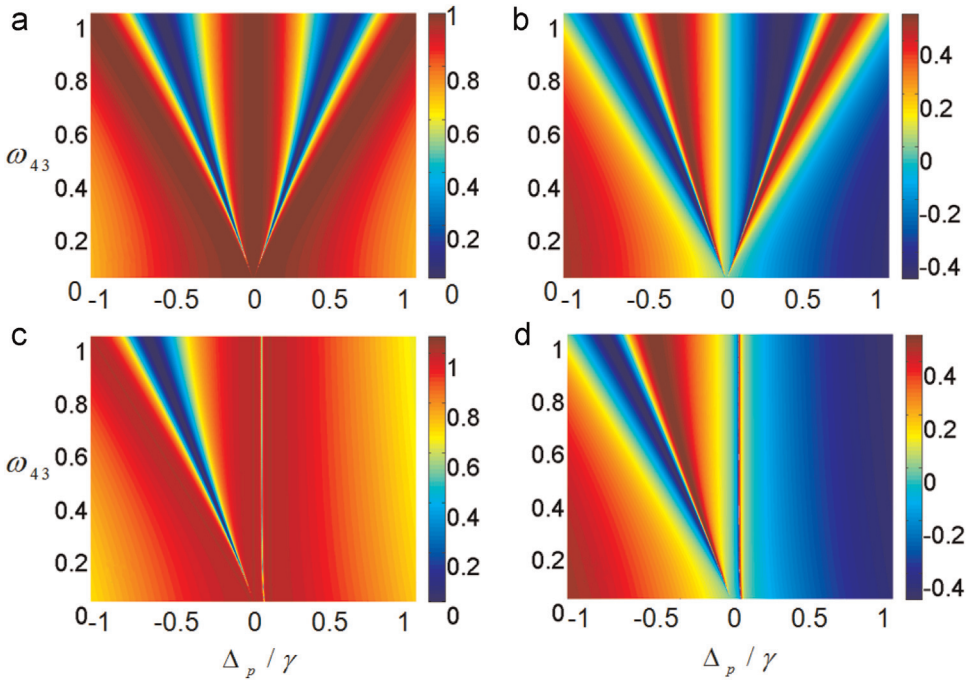

Fig. 3. (a) and (c) are the absorption spectrum as functions of Δ_p and ω_{43}, (b) and (d) are the dispersion spectrum as functions of Δ_p and ω_{43}. (a) and (b) $p = 1$, $\omega_{32} = \omega_{43}$. (c) and (d) $p = 1$, $\omega_{32} = 0.1$. Other parameters are the same as those in Fig. 2.

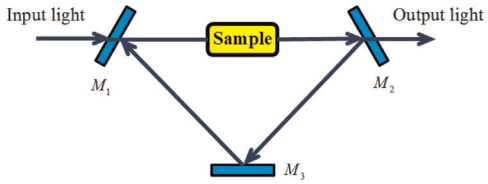

Fig. 4. The schematic of an atomic-cavity system.

becomes much narrower, and at the same time the position of them moves to the center of the spectrum. And the narrower transmission peaks are due to the steeper dispersion within the narrower transparency windows [Fig. 2(c)]. The transmission spectrum goes to unsymmetrical when the frequency splitting $\omega_{32} \neq \omega_{43}$, as shown in Fig. 5(d). And also the smaller value of frequency splitting results in the narrower linewidth of the transmission peak.

So it can be concluded that SGC is responsible for the appearance of transmission peaks. Besides, the frequency splitting can modify both the linewidth and the position of the transmission peaks. With reduced value of frequency splitting, the transmission peaks move to the center of the spectrum, and the linewidth of the transmission peaks is narrowed. For equal small value of frequency splitting, one can simultaneously obtain two narrow transmission peaks.

We also plot in Fig. 6 the three dimensional transmission spectrum for various value of frequency splitting ω_{32} and ω_{43} with the same parameters used in Fig. 3. When $\omega_{32} = \omega_{43}$, the transmission spectrum is symmetrical with two transmission peaks. And with decreasing value of ω_{43}, the linewidth of the two transmission peaks becomes narrowing, and at the same time the position of them is moving to the center of the spectrum [Fig. 6 (a)]. As for the different frequency splitting $(\omega_{32} \neq \omega_{43})$, the transmission spectrum is unsymmetrical. The width of one transmission peak is kept narrowed, and the position of it is

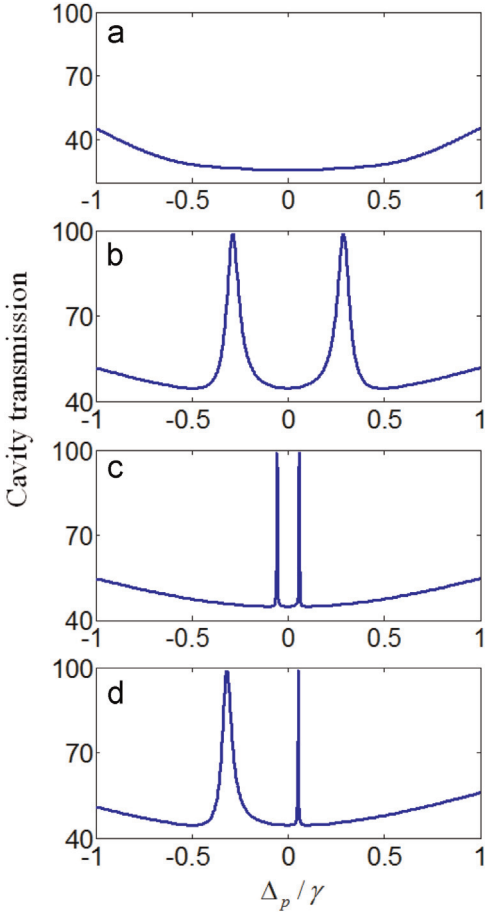

Fig. 5. The cavity transmission spectrum as a function of Δ_p. The parameters refer to Fig. 2, and $r = 0.98$, $L = 20$ cm and $N\sigma_{10}l = 0.5$.

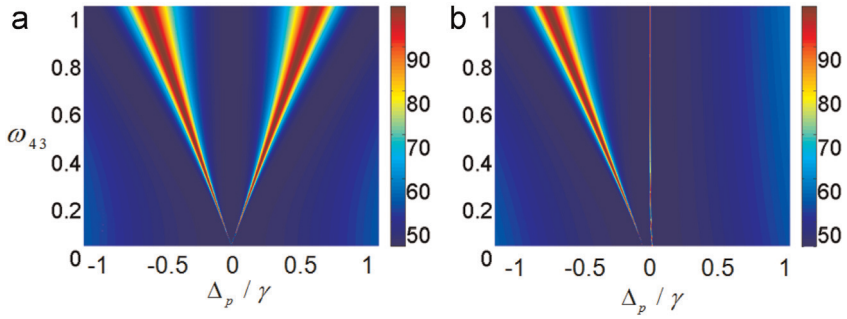

Fig. 6. The cavity transmission spectrum as functions of Δ_p and ω_{43} for $p = 1$. (a) $\omega_{32} = \omega_{43}$, (b) $\omega_{32} = 0.1$. Other parameters are the same as those in Fig. 2, and $r = 0.98$, $L = 20$ cm and $N\sigma_{10}l = 0.5$.

unchanged. With reduced value of ω_{43}, the width of other transmission peak can also acquire linewidth narrowing [Fig. 6(b)].

5. Conclusions

In conclusion, we proposed a scheme for obtaining a tunable ultranarrow cavity transmission controlled by SGC. Due to SGC, two transparency windows are obtained. And by proper tuning the frequency splitting, the transparency windows can be made very narrow, and within the narrow transparency windows steep dispersion can be acquired. Furthermore, when the sample is embedded in a ring cavity, ultranarrow transmission peaks can be obtained close to the transparency frequency. And for equal small value of frequency splittings, two ultranarrow transmission peaks can be obtained simultaneously. The cavity-linewidth narrowing is due to the steep dispersion and reduced absorption produced by SGC, requiring no coupling lasers.

Finally, it should be emphasized that, the existence of SGC needs for near-degenerate closely spaced levels with non-orthogonal dipole moments and these conditions are rarely met in real atoms. However this type of quantum interference can be observed in many incoherent decay processes. When an atom is coupled to the modified vacuum [38–41], quantum interference occurs even if the corresponding dipole moments are orthogonal. And SGC can also be simulated by additional fields in the dressed-state picture [42–48]. Moreover, the tunneling effect in quantum wells and quantum dots can also lead to quantum interference [49–52]. Therefore, the scheme proposed here can be equally applied to the above systems where SGC exists.

Acknowledgments

This work is supported by the financial support from the National Natural Science Foundation of China (Grant nos. 11304308, 11204029, 61306086, 61176046 and 61404138), the National Basic Research Program of China (Grant nos. 2013CB933300), the International Science Technology Cooperation Program of China (No. 2013DFR00730), Jilin Provincial Natural Science Foundation (Grant nos. 20140101203JC and 20140520127JH).

References

[1] S.E. Harris, Phys. Today 52 (1997) 36.
[2] M. Fleischhauer, A. Imamoglu, J.P. Marangos, Rev. Mod. Phys. 77 (2005) 633.
[3] L.V. Hau, S.E. Harris, Z. Dutton, C.H. Behroozi, Nature 397 (1999) 594.
[4] M.M. Kash, V.A. Sautenkov, A.S. Zibrov, L. Hollberg, G.R. Welch, M.D. Lukin, Y. Rostovtsev, E.S. Fry, M.O. Scully, Phys. Rev. Lett. 82 (1999) 5229.
[5] M. Fleischhauer, M.D. Lukin, Phys. Rev. Lett. 84 (2000) 5094.
[6] S.E. Harris, L.V. Hau, Phys. Rev. Lett. 82 (1999) 4611.
[7] M.D. Lukin, M. Fleischhauer, M.O. Scully, V.L. Velichansky, Opt. Lett. 23 (1998) 295.
[8] H. Wang, D.J. Goorskey, W.H. Burkett, M. Xiao, Opt. Lett. 25 (2000) 1732.
[9] G. Hernandez, J.P. Zhang, Y.F. Zhu, Phys. Rev. A 76 (2007) 053814.
[10] H. Wu, J. Gea-Banacloche, M. Xiao, Phys. Rev. Lett. 100 (2008) 173602.
[11] K. Ying, Y.P. Niu, D.J. Chen, H.W. Cai, R.H. Qu, S.Q. Gong, J. Opt. Soc. Am. B 31 (2014) 144.
[12] J.P. Zhang, G. Hernandez, Y.F. Zhu, Opt. Lett. 33 (2008) 46.
[13] G.S. Agarwal, Quamtum Optics. Springer Tracts in Modern Physics, Spriger-Verlag, Berlin, 1974.
[14] S.Y. Zhu, R.C.F. Chan, C.P. Lee, Phys. Rev. A 52 (1995) 710.
[15] S.Y. Zhu, M.O. Scully, Phys. Rev. Lett. 76 (1996) 388.
[16] P. Zhou, S. Swain, Phys. Rev. Lett. 77 (1996) 3995.
[17] E. Paspalakis, P.L. Knight, Phys. Rev. Lett. 81 (1998) 293.
[18] J.H. Wu, A.J. Li, Y. Ding, Y.C. Zhao, J.Y. Gao, Phys. Rev. A 72 (2005) 023802.
[19] I. Gonzalo, M.A. Antón, F. Carreño, O.G. Calderón, Phys. Rev. A 72 (2005) 033809.
[20] S.E. Harris, Phys. Rev. Lett. 62 (1989) 1033.
[21] A. Imamoğlu, Phys. Rev. A 40 (1989) 2835.
[22] J.H. Wu, J.Y. Gao, Phys. Rev. A 65 (2002) 063807.
[23] S.C. Tian, R.G. Wan, Z.H. Kang, H. Zhang, Y. Jiang, H.N. Cui, J.Y. Gao, J. Opt. Soc. Am. B 29 (2012) 881.
[24] P. Zhou, S. Swain, Phys. Rev. Lett. 78 (1997) 832.
[25] E. Paspalakis, N.J. Kylstra, P.L. Knight, Phys. Rev. Lett. 82 (1999) 2079.
[26] A. Joshi, W.G. Yang, Min Xiao, Phys. Rev. A 68 (2003) 015806.
[27] M.A. Antón, Oscar G. Calderón, F. Carreño, Phys. Lett. A 311 (2003) 297.
[28] D.C. Cheng, C.P. Liu, S.Q. Gong, Phys. Lett. A 332 (2004) 244.
[29] K.I. Osman, A. Joshi, Phys. Lett. A 376 (2012) 2565.
[30] S. Aas, Ö.E. Müstecaplıoğlu, Phys. Rev. A 88 (2013) 053846.
[31] Y.P. Niu, S.Q. Gong, Phys. Rev. A 73 (2006) 053811.
[32] R.G. Wan, J. Kou, L. Jiang, Y. Jiang, J.Y. Gao, Phys. Rev. A 83 (2011) 033824.
[33] M.O. Scully, Phys. Rev. Lett. 104 (2010) 207701.
[34] O. Postavaru, Z. Harman, C.H. Keitel, Phys. Rev. Lett. 106 (2011) 033001.
[35] K.I. Osman, A. Joshi, Eur. Phys. J. D (2014).
[36] M.A. Antón, O.G. Calderón, F. Carreño, Phys. Rev. A 72 (2005) 023809.
[37] A. Fountoulakis, A.F. Terzis, E. Paspalakis, Phys. Rev. A 73 (2006) 033811.
[38] A.K. Patnaik, G.S. Agarwal, Phys. Rev. A 59 (1999) 3015.
[39] G.S. Agarwal, Phys. Rev. Lett. 84 (2000) 5500.
[40] J.P. Xu, L.G. Wang, Y.P. Wang, Q. Lin, S.Y. Zhu, Opt. Lett. 33 (2008) 2005.
[41] Y.P. Yang, J.P. Xu, H. Chen, S.Y. Zhu, Phys. Rev. Lett. 100 (2008) 043601.
[42] Z. Ficek, S. Swain, Phys. Rev. A 69 (2004) 023401.
[43] J.H. Li, J.B. Liu, A.X. Chen Ai-Xi, C.C. Qi, Phys. Rev. A 74 (2006) 033816.
[44] A.J. Li, X.L. Song, X.G. Wei, L. Wang, J.Y. Gao, Phys. Rev. A 77 (2008) 053806.
[45] J.H. Wu, A.J. Li, Y. Ding, Y.C. Zhao, J.Y. Gao, Phys. Rev. A (2005) 023802.
[46] C.L. Wang, Z.H. Kang, S.C. Tian, Y. Jiang, J.Y. Gao, Phys. Rev. A 79 (2009) 043810.
[47] S.C. Tian, Z.H. Kang, C.L. Wang, R.G. Wan, J. Kou, H. Zhang, Y. Jiang, H.N. Cui, J. Y. Gao, Opt. Commun. 285 (2012) 294.
[48] S.C. Tian, C.L. Wang, C.Z. Tong, L.J. Wang, H.H. Wang, X.B. Yang, Z.H. Kang, J. Y. Gao, Opt. Exp. 20 (2012) 23559.
[49] J.H. Wu, J.Y. Gao, J.H. Xu, L. Silvestri, M. Artoni, G.C. LaRocca, F. Bassani, Phys. Rev. Lett. 95 (2005) 057401.
[50] J.H. Li, Phys. Rev. B 75 (2007) 155329.
[51] S.C. Tian, C.Z. Tong, C.L. Wang, L.J. Wang, H. Wu, E.B. Xing, Y.Q. Ning, L.J. Wang, Opt. Commun. 312 (2014) 296.
[52] S.C. Tian, C.Z. Tong, C.L. Wang, Y.Q. Ning, J. Lumin. 153 (2014) 169.